ISSN 0015-4628, Fluid Dynamics, 2023, Vol. 58, No. 5, pp. 942–959. © The Author(s), 2023. This article is an open access publication.
Russian Text © The Author(s), 2023, published in Izvestiya RAN. Mekhanika Zhidkosti i Gaza, 2023, No. 5, pp. 119–137.

Radiative–Convective Heating of the Surface of the Martian Descent Vehicle MSL with Taking into Account the Turbulent Nature of Flow

S. T. Surzhikov[a,*]

[a] *Ishlinsky Institute for Problems in Mechanics, Russian Academy of Sciences, Moscow, Russia*

**e-mail: surg@ipmnet.ru*

Received June 2, 2023; revised June 6, 2023; accepted June 6, 2023

Abstract—The three-dimensional computer model based on the Reynolds-averaged Navier–Stokes equations together with the Baldwin–Lomax and Prandtl algebraic models of turbulent mixing is used to calculate radiative–convective heat transfer on the surface of the MSL descent space vehicle. The intensification of convective heat transfer on the leeward side of the frontal aerodynamic shield and the superiority of the radiative heat flux density over the convective one on the rear surface are demonstrated. The calculations are performed using the physically and chemically nonequilibrium gas model. The results are compared with the calculations based on other computational models and the flight data on the heat load to the descent vehicle obtained during MSL descent in the dense layers of the Martian atmosphere.

Keywords: radiative gas dynamics, convective surface heating, turbulent boundary layer, Reynolds-averaged Navier–Stokes equations, algebraic turbulence models

DOI: 10.1134/S0015462823601262

In [1], the calculated and flight experimental data testifying that laminar–turbulent transition (LTT) takes place on the frontal aerodynamic shield of the Mars Science Laboratory (MSL) descent vehicle (DV) are discussed. A significant interest of specialists in this problem arose due to the fact that the aerodynamic shield of the MSL descent vehicle had a diameter D of 4.5 m, which significantly exceeded the dimensions of the aerodynamic shields of previously implemented space missions, namely, the Viking descent vehicle had $D = 3.5$ m, the Pathfinder, the Mars Exploration Rover, and the Mars Phoenix descent vehicles had $D = 2.5$ m [2]. Taking into account not only the characteristic dimensions, but also specific flight conditions, an analysis of aerothermodynamics of these descent vehicles showed that for the MSL spacecraft, the laminar–turbulent transition can be observed on the leeward side of the frontal aerodynamic shield before the peak thermal load is reached [3]. For the smaller descent vehicles, laminar–turbulent transition was not assumed until the instant of the maximum thermal load. Unfortunately, this fact was not experimentally confirmed for previous Martian landers.

The post-flight analysis of the results of temperature measurements in the subsurface layers of thermal protection [1] confirmed the existence of expected laminar–turbulent transition on the leeward surface of the frontal aerodynamic shield. A detailed analysis of the obtained experimental flight data also raised a number of additional questions about the role of surface roughness of the thermally decomposed heat-shielding material (PICO class—Phenolic Impregnated Carbon Ablator) and even about the contribution of thermal radiation of the compressed layer. Without diminishing the undoubted importance of these factors, in the present paper we will focus on the fundamentally important fact of the presence of laminar-turbulent transition on the frontal aerodynamic shield and its important consequences associated with the intensification of heat transfer in a zone where this is not expected under other conditions. Note an important aspect of its very good prediction in calculations for a real large-scale model of a lander using the LAURA [4] and DPLR [5] computer codes, in which the Reynolds-averaged Navier–Stokes equations (RANS models) are implemented together with algebraic turbulence models. Unfortunately, the numerical details of these calculations were not given in [1].

In [1], the good quality of prediction of experimental data on convective heating in laboratory tests of the MSL scale model using the LAURA code was also noted. In [6], it was also demonstrated a good agreement with the mentioned laboratory experimental data of the results of calculations using the

NERAT-3D computer code, in which the RANS model is implemented together with the Baldwin–Lomax algebraic turbulence models [7, 8] and the Prandtl mixing model [9]. The present paper demonstrates the results of the development of this model in relation to the interpretation of flight experimental data [1] for a large-scale model under real conditions of hypersonic braking in the dense layers of the Martian atmosphere. The aspects of accounting for nonequilibrium physical and chemical processes and transfer of selective thermal radiation are also touched upon.

We especially note that although in the problems of aerophysics of reentry spacecraft in dense layers of the atmosphere it is often difficult to identify the determining processes, which, moreover, can replace each other at different phases of the deceleration trajectory, the phenomenon of laminar-turbulent transition and turbulent heating of the vehicle surface is one from the key ones. The hypersonic velocities of the descent vehicles and their large sizes lead to intense convective heating of vast surfaces, which is a great problem for maintaining the safe thermal balance. The phenomenon of LTT leads to the need to change the structure of the thermal protection of the descent vehicles.

The specific feature of the study of turbulent heating of extended surfaces at hypersonic velocities is the fact that the gradients of gas-dynamic quantities sharply increase after LTT in the turbulent flow region. A detailed theoretical substantiation of this fact is given in monograph [10]. Computer simulation of an already time-consuming three-dimensional (spatial) problem becomes even more complicated due to the need to take into account the near-wall structure of the turbulent boundary layer. The reliability of the obtained calculated data on the intensity of convective heating depends in great extent on the accuracy of description of this structure.

Turbulent heating of the extended surface of frontal aerodynamic shield of the descent vehicle has a number of other features associated with the destruction of thermal protection and non-equilibrium physical and chemical processes in the compressed layer and in the near-surface layers of the destructible material. A significant uncertainty in the calculated data obtained is associated with a model description of catalysis on the surface (especially on a thermally destroyed one). Another source of reliability reduction is related to the fact that in a chemically reacting compressed layer the diffusion component of the convective heat flux can exceed the thermal conductivity. However, a model turbulent description of mass transfer near the surface is traditionally a more complex and less formalized problem. As an illustration of this statement, we note that the data on the total convective heating of the MSL frontal aerodynamic shield in [1], obtained from two (not very different) models of surface catalyticity, differ quite noticeably. Another important aspect of the numerical simulation of turbulent heating is associated with the uncertainty of the influence of surface roughness, whose inclusion or disregard can be considered as one of the objective reasons for the deviation of the calculated data from the experimental ones.

In the present paper, the model of radiation gas dynamics of reentry spacecraft, implemented in the author's computer code NERAT-3D, which was used in the laminar flow calculation regime to study the aerophysics of Martian [11–15] and reentry spacecraft returning to Earth [16], is developed in part taking into account the turbulent convective heating of the frontal aerodynamic shield for the conditions of actual deceleration of the MSL descent vehicle in the Martian atmosphere. The three-dimensional nature of the flow of physically and chemically nonequilibrium carbon dioxide with the formation of a turbulent boundary layer is considered. The surface is assumed to be smooth and catalytic, and the number densities of the components of partially dissociated carbon dioxide on the surface are determined from local equilibrium conditions.

Determination of the gas-dynamic characteristics of the three-dimensional flow makes it possible to calculate the heating of the surface of the descent vehicle by selective thermal radiation. The calculations show that in the case of the MSL descent vehicles the heating of individual parts of the surface by thermal radiation is more significant than by convective heat transfer.

Taking into account the large deficit of nodes of the used finite-difference grid, it is necessary to keep in mind the low reliability of determining the density of the convective heat flux on the back surface of the descent vehicle. Radiative heat transfer in the problems under consideration is of the volumetric nature, so the detail of the grid near the rear surface is not fundamentally important. If necessary, a specially constructed grid with clusters of nodes in the required flow regions should be used.

1. NUMERICAL MODEL

For the purposes of subsequent analysis, it is convenient to conditionally divide the system of integrable equations into four groups:

– system of gas dynamics equations,

– system of physical and chemical kinetics equations,

– system of multigroup equations for transfer of selective thermal radiation,

– equations of the turbulent mixing model.

For the purpose of practical implementation of numerical integration of a very complex system of conjugate nonlinear partial derivative equations, moreover, in the case of three spatial variables and, what is fundamentally important, in the presence of regions of the boundary layers with large gradients of unknown functions, special numerical procedures must be applied to solve the problem of integrating each of the marked blocks of equations. We will explain the specifics of the equations of each of the distinguished groups.

The system of gas-dynamic equations is composed of the continuity equations for the mixture of gases and the Navier–Stokes equations in the form of the Reynolds-averaged equations with the use of the Boussinesq hypothesis:

$$\frac{\partial \rho}{\partial t} + \frac{\partial \rho u}{\partial x} + \frac{\partial \rho \upsilon}{\partial y} + \frac{\partial \rho w}{\partial z} = 0, \tag{1.1}$$

$$\frac{\partial \rho u}{\partial t} + \operatorname{div}(\rho u \mathbf{V}) = -\frac{\partial p}{\partial x} + \Pi_{x,\text{eff}}, \tag{1.2}$$

$$\frac{\partial \rho \upsilon}{\partial t} + \operatorname{div}(\rho \upsilon \mathbf{V}) = -\frac{\partial p}{\partial r} + \Pi_{y,\text{eff}}, \tag{1.3}$$

$$\frac{\partial \rho w}{\partial t} + \operatorname{div}(\rho w \mathbf{V}) = -\frac{\partial p}{\partial z} + \Pi_{z,\text{eff}}, \tag{1.4}$$

where the components of the viscous stress tensor can be expressed as follows:

$$\Pi_{x,\text{eff}} = -\frac{2}{3}\frac{\partial}{\partial x}(\mu_{\text{eff}} \operatorname{div}\mathbf{V}) + 2\frac{\partial}{\partial x}\left(\mu_{\text{eff}}\frac{\partial u}{\partial x}\right) + \frac{\partial}{\partial y}\left[\mu_{\text{eff}}\left(\frac{\partial \upsilon}{\partial x} + \frac{\partial u}{\partial y}\right)\right] + \frac{\partial}{\partial z}\left[\mu_{\text{eff}}\left(\frac{\partial w}{\partial x} + \frac{\partial u}{\partial z}\right)\right],$$

$$\Pi_{y,\text{eff}} = -\frac{2}{3}\frac{\partial}{\partial y}(\mu_{\text{eff}} \operatorname{div}\mathbf{V}) + 2\frac{\partial}{\partial y}\left(\mu_{\text{eff}}\frac{\partial v}{\partial y}\right) + \frac{\partial}{\partial x}\left[\mu_{\text{eff}}\left(\frac{\partial \upsilon}{\partial x} + \frac{\partial u}{\partial y}\right)\right] + \frac{\partial}{\partial z}\left[\mu_{\text{eff}}\left(\frac{\partial w}{\partial y} + \frac{\partial \upsilon}{\partial z}\right)\right],$$

$$\Pi_{z,\text{eff}} = -\frac{2}{3}\frac{\partial}{\partial z}(\mu_{\text{eff}} \operatorname{div}\mathbf{V}) + 2\frac{\partial}{\partial z}\left(\mu_{\text{eff}}\frac{\partial w}{\partial z}\right) + \frac{\partial}{\partial x}\left[\mu_{\text{eff}}\left(\frac{\partial w}{\partial x} + \frac{\partial u}{\partial z}\right)\right] + \frac{\partial}{\partial y}\left[\mu_{\text{eff}}\left(\frac{\partial w}{\partial y} + \frac{\partial \upsilon}{\partial z}\right)\right],$$

where u, υ, w are the projections of the flow velocity vector $\mathbf{V}$ on the axes of the rectangular Cartesian coordinate system x, y, z; p, ρ, and T are the pressure, the density, and the temperature of the gas; $\mu, \lambda, \mu_t, \lambda_t, \mu_{\text{eff}} = \mu + \mu_t, \lambda_{\text{eff}} = \lambda + \lambda_t$ are the molecular, turbulent and effective viscosities and the thermal conductivities.

The second group consists of the energy conservation equations for the translational degrees of freedom of gas particles and the vibrational degrees of freedom of the O_2, CO, and CO_2 molecules, as well as the continuity equations for each component of the gas mixture:

$$\rho c_p \frac{dT}{dt} = \operatorname{div}\left(\lambda_{\text{eff}} \operatorname{grad} T - \sum_{i=1}^{N_s} h_i \mathbf{J}_i - \mathbf{q}_R\right) + \frac{dp}{dt} + \Phi_\mu + Q_{\text{vib}} - \sum_{i=1}^{N_s} h_i \dot{w}_i, \tag{1.5}$$

$$\frac{d\rho_i}{dt} + \rho_i \operatorname{div}\mathbf{V} = -\operatorname{div}\mathbf{J}_i + \dot{w}_i, \quad i = 1, 2, \ldots, N_s, \tag{1.6}$$

$$\frac{d\rho e_{v,m}}{dt} + \rho e_{v,m} \operatorname{div}(\mathbf{V}) = \operatorname{div}(-\mathbf{J}_m e_{v,m}) + \dot{e}_{v,m}, \quad m = 1, 2, \ldots, N_V, \tag{1.7}$$

where T is the temperature of the translational degrees of freedom; μ and λ are the viscosity and thermal conductivity coefficients, c_p is the specific heat capacity at constant pressure, $c_p = \sum_i^{N_s} Y_i c_{p,i}$, $Y_i = \rho_i/\rho$ is the mass fraction of the ith component of flow; $c_{p,i}$ and h_i are the specific heat capacity of translational and rotational degrees of freedom at constant pressure and the specific enthalpy of the ith flow component; D_i is the effective diffusion coefficient of the ith component of flow; ρ_i and $\mathbf{J}_i$ are the density and mass diffusion flux of the ith flow component; $\mathbf{J}_i = -\rho D_i \operatorname{grad} Y_i$, N_s is the number of the gas mixture

components (C, O, C_2, O_2, CO, and CO_2); $e_{v,m}$ is the specific vibrational energy of the mth vibrational mode of the ith flow component (the vibrational modes of the O_2 and CO molecules are taken into account, as well as three vibrational modes of a CO_2 molecule, namely, the deformation, symmetric, and antisymmetric modes); $\dot{e}_{v,m}$ is the rate of variation in the specific vibrational energy in the mth vibrational mode; Q_{vib} is the total thermal effect of the vibrational relaxation processes determined by solving the system of equations (1.7); $\rho_{i(m)}$ is the density of the ith flow component that has the mth vibrational mode; $e^0_{v,m} = e_{v,m}(T_V = T)$ is the equilibrium specific energy of vibrations of the mth mode of the ith flow component; $T_{V,m}$ is the temperature in the mth vibrational mode of the ith flow component, and the dissipative function is

$$\Phi_\mu = \mu_{\text{eff}}\left[2\left(\frac{\partial u}{\partial x}\right)^2 + 2\left(\frac{\partial \upsilon}{\partial y}\right)^2 + 2\left(\frac{\partial w}{\partial z}\right)^2 + \left(\frac{\partial v}{\partial x} + \frac{\partial u}{\partial y}\right)^2 + \left(\frac{\partial w}{\partial y} + \frac{\partial \upsilon}{\partial z}\right)^2 + \left(\frac{\partial u}{\partial z} + \frac{\partial w}{\partial x}\right)^2 - \frac{2}{3}\left(\frac{\partial u}{\partial x} + \frac{\partial \upsilon}{\partial y} + \frac{\partial w}{\partial z}\right)^2\right]. \tag{1.8}$$

The direct connection between the first and second groups of equations is implemented by the thermal and caloric equations of state of an ideal gas

$$p = \rho\frac{R_0}{M_\Sigma}T = \rho R_0 T\sum_i^{N_s}\frac{Y_i}{M_i}, \tag{1.9}$$

$$e = \int_{T_0}^{T} c_v dT + e_0, \tag{1.10}$$

where $R_0 = 8.314\times10^7$ erg/(K mol) is the universal gas constant, e_0 is the internal energy at a certain temperature T_0 (defined in different ways in thermodynamic databases, for example, $T_0 = 273$ K), and M_i is the molecular weight of the ith component of the gas mixture. Note that in problems of physical gas dynamics, the equations of type (1.6) are assigned to the class of equations of chemical kinetics, and equations (1.7) to the class of equations of physical kinetics.

Taking into account the fact that vibrational excitation of molecules may differ from the equilibrium one, the specific internal energy can be written in the form (taking into account the linearity of the triatomic CO_2 molecule):

$$e_i = \frac{3}{2}R_i T + R_i T + R_i\sum_m \frac{\theta_{m(i)}}{\exp\left(-\dfrac{\theta_{m(i)}}{T_{V,m(i)}}\right)-1}, \tag{1.11}$$

where it is assumed that the internuclear potential of form of a harmonic oscillator is used. Here, $\theta_{m(i)}$ are the characteristic vibrational temperatures that determine the specific vibrational energy for each mode, and R_i is the molecular gas constant.

In Eq. (1.7) we used the following relations:

$$\dot{e}_{v,m} = \rho_{i(m)}\frac{e^0_{v,m} - e_{v,m}}{\tau_m} - Q^m_{CV}, \tag{1.12}$$

$$e_{v,m} = \frac{R_0\theta_m}{M_{i(m)}\left[\exp\left(\theta_m/T_{v,m}\right)-1\right]}, \tag{1.13}$$

where equation (1.12) expresses the rate of variation in the specific vibrational energy in the mth vibrational mode due to vibrational-translational (VT) relaxation and due to chemical reactions (CV), τ_m is the vibrational relaxation time of the molecule in a given vibrational mode.

In accordance with the adiabatic theory, the characteristic time of particle-to-particle collisions τ_c should be significantly greater than the characteristic period of molecular vibrations τ_V. However, as shown in [17], at high temperatures ($T > 10000$ K) this condition is not satisfied, because the time between

collisions becomes so small that $\tau_c/\tau_V \sim 1$. The deviation from the conditions of the adiabatic theory leads to an incorrect underestimation of the vibrational relaxation time. This was the reason why Park [18] introduced a restriction from below on the VT relaxation time. Therefore, the VT relaxation time $\tau_{VT,i}$ was calculated according to the recommendations of Millikan and White [19] with Park's correction, which bounds the value of $\tau_{VT,i}$ from below

$$\tau = \tau_{VT} + \frac{1}{N_t \sigma_V \sqrt{8kT/(\pi M_m)}}, \quad \sigma_V = \sigma'_V \left(50000/T\right)^2, \tag{1.14}$$

$$p\tau_{VT} = \exp[A_{VT}(T^{-1/3} - B_{VT}) - 18.42], \tag{1.15}$$

$$A_{VT} = 0.00116\mu^{0.5}\theta_V^{1.333}, \quad B_{VT} = 0.015\mu^{0.25}. \tag{1.16}$$

$$\sigma'_V = 3\times 10^{-17}\ \text{cm}^2.$$

The definition of partial relaxation times makes it possible to set the vibrational relaxation time for a given vibrational mode in a gas mixture as follows:

$$\tau_m = \left(\sum_{i=1}^{N} \frac{x_i}{\tau_{m,i}}\right)^{-1}. \tag{1.17}$$

The change in the vibrational energy due to the occurrence of chemical reactions was taken into account using a simple model:

$$Q_{CV}^m = e_{V,m}\frac{1}{2}\left(\dot{w}_{i(m)} - \left|\dot{w}_{i(m)}\right|\right), \tag{1.18}$$

where it was assumed that the decrease in the vibrational energy in the mth mode by 1 cm^3 per 1 s is proportional to the volume rate of disappearance of molecules that have this vibrational mode.

Diffusion energy transfer of the vibrational excitation of molecules was taken into account due to their diffusion, that is, the vibrational energy flux density due to diffusion was determined from the formula

$$e_{i,m}\mathbf{J}_{D,v,i} = -e_{i,m}\rho D_{v,i}\,\text{grad}\,Y_i, \tag{1.19}$$

where $D_{V,i}$ is the effective diffusion coefficient of the vibrational excitation energy which was taken to be equal to the effective diffusion coefficient equal to the sum of the molecular and turbulent diffusion coefficients $D_{V,i} = D_i + D_t$.

The used models of chemical kinetics of a multicomponent gas mixture were formulated in canonical form for each chemical reaction (the complete set of chemical reactions taken into account is given in [16])

$$\sum_{j=1}^{N_s} a_{j,n}[X_j] = \sum_{j=1}^{N_s} b_{j,n}[X_j], \quad n = 1,2,\ldots,N_r, \tag{1.20}$$

then the rate of formation of the ith component in the nth chemical reaction can be written in the form:

$$\left(\frac{\mathrm{d}X_i}{\mathrm{d}t}\right)_n = k_{f,n}\left(b_{i,n} - a_{i,n}\right)\prod_j^{N_s} X_j^{a_{j,n}} - k_{r,n}\left(b_{i,n} - a_{i,n}\right)\prod_j^{N_s} X_j^{b_{j,n}} = \left(b_{i,n} - a_{i,n}\right)\left(S_{f,n} - S_{r,n}\right), \tag{1.21}$$

where $a_{i,n}$ and $b_{i,n}$ are the stoichiometric coefficients of the nth chemical reaction; X_i is the volume-molar concentration of the ith component; $[X_j]$ are the chemical symbols of reagents and products of chemical reactions; N_r is the number of chemical reactions; $S_{f,n}$ and $S_{r,n}$ are the forward and reverse reaction rates; and $k_{f,n}$ and $k_{r,n}$ are the rate constants of the forward and reverse reactions.

The mass rate of formation of the ith component per unit volume is determined as follows:

$$\dot{w}_i = M_i\sum_{n=1}^{N_r}\left(b_{i,n} - a_{i,n}\right)\left(S_{f,n} - S_{r,n}\right), \frac{\text{g}}{\text{cm}^3\text{s}}. \tag{1.22}$$

From (1.21) it follows that in order to calculate the mass rate of formation of the ith component, it is necessary to determine the rate constants of the forward and reverse reactions for each of the N_r reactions. These constants were approximated by the generalized Arrhenius dependence

$$k_{f(r),n} = A_{f(r),n} T^{n_{f(r),n}} \exp\left(-\frac{E_{f(r),n}}{kT}\right), \tag{1.23}$$

where $A_{f(r),n}, n_{f(r),n}$ and $E_{f(r),n}$ are the approximating coefficients for the rate constants of the forward (f) and reverse (r) chemical reactions; and T is the temperature of the translational degrees of freedom. Within the framework of the model used, the temperature of rotational motion is considered to be equal to the temperature of translational motion, k is the Boltzmann constant, and n is the number of chemical reaction in the kinetic model. The condition of quasi-neutrality was used to find the molar electron concentrations.

The catalytic surface model was used; according to this model, the mass fractions of the mixture components $(Y_i)_w$ were found from the condition of thermodynamic equilibrium. The surface temperature was either set constant or calculated using the condition

$$\varepsilon\sigma T_w^4 = Q_w, \tag{1.24}$$

where ε is the emissivity factor of the surface ($\varepsilon = 0.8$); $\sigma = 5.67\times10^{-12}$ W/(cm^2 K^4) is the Stefan–Boltzmann constant; and q_w is the density of the heat flux incident on the surface.

The solution of the equations of physical (1.7) and chemical (1.6), (1.21) kinetics makes it possible to modify the dissociation rate constants of molecular components using the Treanor–Marrone model [20]. The dissociation rate constants $k_f = k_D$ used in the calculations were modified to take into account thermal nonequilibrium of the molecules

$$k_D(T,T_V) = k_D(T)\, Z(Q_T, Q_V, Q_m), \tag{1.25}$$

$$Z(Q_T, Q_V, Q_m) = \frac{Q(T)Q(T_m)}{Q(T_V)N}, \tag{1.26}$$

where N is the number of vibrational levels calculated as follows:

$$N = \left[\frac{D_0}{\Delta E_V}\right],$$

where ΔE_V is the energy difference between two successive levels (remains constant within the harmonic oscillator model).

The statistical sums are calculated using the relations

$$Q_{T_*} = \frac{1-e^{-D_0/T_*}}{1-e^{-\theta_V/T_*}} e^{-\theta_V/2T_*}, \quad T_* = T,\ T_V, \tag{1.27}$$

$$Q_m = \frac{\theta_V}{D_0}\frac{1-e^{-D_0/T_m}}{1-e^{-\theta_V/T_m}} e^{-\theta_V/2T_m}, \quad T_m = \frac{TT_V}{T-T_V}. \tag{1.28}$$

The transport, thermodynamic, and thermophysical characteristics were set as follows. The transport properties of the multicomponent gas (the viscosity, thermal conductivity, and diffusion coefficients) are calculated in the first approximation of the Chapman–Enskog theory [21, 22]

$$\mu_i = 2.67\times10^{-5}\frac{\sqrt{M_i T}}{\sigma_i^2 \Omega_i^{(2,2)*}},\ \text{g/cm s}, \quad \lambda_i = 8330\sqrt{\frac{T}{M_i}}\frac{1}{\sigma_i^2\Omega_i^{(2,2)*}},\ \text{erg/cm K}, \tag{1.29}$$

where σ_i is the effective collision diameter, Å, $\Omega_i^{(2,2)*} = f(T_i)$ is the collision integral, $T_i = kT/\varepsilon_i$, ε_i/k is a parameter characterizing the depth of the potential energy of interaction of particles of the ith kind, as well as with the use of the approximate combinatorial Mann–Brockau and Wilke relations [23, 24], which make it possible to calculate the properties necessary for the computational model

$$\mu = 1\Big/\sum_{i=1}^{N_s}\left(\frac{Y_i}{\mu_i}\right), \quad \lambda = \frac{1}{2}\left[\sum_{i=1}^{N_s} x_i\lambda_i + 1\Big/\sum_{i=1}^{N_s}\left(\frac{x_i}{\lambda_i}\right)\right],$$

$$D_i = \frac{1 - x_i}{\sum\limits_{j \neq i}^{N_s} (x_j / D_{i,j})}, \quad D_{i,j} = 1.858 \times 10^{-3} \sqrt{T^3 \frac{M_i + M_j}{M_i M_j}} \frac{1}{p \sigma_{i,j}^2 \Omega_{i,j}^{(1,1)*}}, \text{ cm}^2/\text{s}. \tag{1.30}$$

The collision integrals are calculated using the approximations proposed by Anfimov [25]

$$\Omega_i^{(2,2)*} = 1.157 T_i^{-0.1472}, \quad \Omega_{i,j}^{(1,1)*} = 1.074 T_{i,j}^{-0.1604}, \tag{1.31}$$

where the functions that determine the collisions of two particles are determined by the so-called combinatorial formulas

$$T_{i,j} = \frac{kT}{\varepsilon_{i,j}}, \quad \varepsilon_{i,j} = \sqrt{\varepsilon_i \varepsilon_j}, \quad \sigma_{i,j} = \frac{1}{2}(\sigma_i + \sigma_j). \tag{1.32}$$

In the initial stage of integration of the complete system of equations, the perfect gas model was used. According to this model we have:

$$\gamma = c_p / c_v = 1.15, \quad c_v = \frac{R_0}{(\gamma - 1)M}, \quad \mu = \frac{1.384 \times 10^{-4}}{274 + T} \left(\frac{T}{273} \right)^{1.5} \text{ g}/(\text{cm s}), \tag{1.33}$$

$$\lambda = \mu c_p / \text{Pr}, \quad \lambda_t = \mu_t c_p / \text{Pr}_t, \quad \text{Pr} = 0.7, \quad \text{Pr}_t = 1.0.$$

The multigroup equation for transfer of selective thermal radiation was integrated to determine the density of the radiative heat flux on the surface of the descent vehicle. The radiative transfer equation with respect to the spectral intensity of radiation was formulated in general form for a nonscattering medium

$$\mathbf{\Omega} \frac{\partial J_\omega(\mathbf{r}, \mathbf{\Omega})}{\partial \mathbf{r}} + \kappa_\omega(\mathbf{r}) J_\omega(\mathbf{r}, \mathbf{\Omega}) = j_\omega(\mathbf{r}). \tag{1.34}$$

After finding the spectral intensity of radiation, the density vector of the integral radiative heat flux and its divergence (which characterizes the volumetric energy balance of thermal radiation) were calculated

$$\mathbf{q}_r = \int\limits_{4\pi} d\Omega \int\limits_{\Delta\omega_{\text{tot}}} J_\omega(\mathbf{r}, \mathbf{\Omega}) \mathbf{\Omega} \, d\omega = \int\limits_{\Delta\omega_{\text{tot}}} \mathbf{q}_{r,\omega}(\mathbf{r}) \, d\omega,$$
$$\mathbf{q}_{r,\omega}(\mathbf{r}) = \int\limits_{4\pi} J_\omega(\mathbf{r}, \mathbf{\Omega}) \mathbf{\Omega} \, d\Omega, \tag{1.35}$$

where $\kappa_\omega(\mathbf{r})$ and $j_\omega(\mathbf{r})$ are the spectral absorption and emission coefficients calculated at local thermodynamic equilibrium using the Kirchhoff law

$$j_\omega(\mathbf{r}) = \kappa_\omega(\mathbf{r}) J_{b,\omega}(\mathbf{r}), \tag{1.36}$$

where $J_{b,\omega}(\mathbf{r})$ is the spectral intensity of radiation of an absolutely black body; $\mathbf{r}$ is the radius vector of a point in space; $\mathbf{\Omega}$ is the unit vector; and $\Delta\omega_{\text{tot}}$ is the spectral range of thermal radiation (in this work 1000–200000 cm^{-1}).

An important characteristic of radiation heating of the descent vehicle is the cumulative function determined for each elementary area on its surface by the following formula:

$$Q_{r,\Delta\omega} = \int\limits_{\omega_{\min}}^{\omega} q_{r,\omega} d\omega, \tag{1.37}$$

where $q_{r,\omega} = (\mathbf{q}_{r,\omega} \cdot \mathbf{n})$ is the density of the spectral flux of thermal radiation on an elementary area with the normal $\mathbf{n}$. The quantity Q_{rad} gives an idea of the fraction of the total radiative heat flux incident on the surface in the spectral range $[\omega_{\min}, \omega]$. At $\omega = \omega_{\max} = 200000$ cm^{-1} Q_{rad} corresponds to the total (integral) heat flux.

The practical implementation of the above computational procedure reduces to the use of the so-called group model of spectral transfer, when the entire spectral range $[\omega_{\min} - \omega_{\max}]$ is divided into N_g inhomogeneous spectral regions of smaller dimensions (in the case under consideration, $N_g = 99$), within each of which all spectral functions are assumed to be independent of the wavelength. We pay special attention to the fact that the differential equation (1.34) is numerically integrated along a sufficiently large number of rays emitted from the surface. To increase the computational efficiency of this procedure, instead of solv-

ing the problems of determining the coordinates of intersection of the emitted ray with the boundaries of elementary computational volumes in the three-dimensional case, the algorithm of quasi-random sampling proposed in [26] is used.

As already noted, the fourth group of equations consists of the equations of algebraic turbulent-mixing models, which have been repeatedly tested in solving problems of practical importance [27]. Two algebraic turbulence models were used. They were repeatedly tested in works on the analysis of turbulent boundary layers. In the first of them, in the Prandtl mixing model [9], the turbulent viscosity is determined from the phenomenological relation

$$\mu_t = \rho L_m^2 |\Omega|, \tag{1.38}$$

where L_m is the Prandtl mixing length and $|\Omega|$ is the velocity vorticity function

$$|\Omega| = \sqrt{\left(\frac{\partial u}{\partial y} - \frac{\partial \upsilon}{\partial x}\right)^2 + \left(\frac{\partial w}{\partial y} - \frac{\partial \upsilon}{\partial z}\right)^2 + \left(\frac{\partial u}{\partial z} - \frac{\partial w}{\partial x}\right)^2},$$

where, in the general case of a boundary layer near a curved surface, by u,v,w we should understand the local velocities along the surface and in normal to it. In this case, a two-layer model is used, according to which the length of the Prandtl mixing path is determined from the formula

$$\begin{gathered} L_m^{\text{in}} = \chi y\left[1 - \exp\left(-\frac{y^+}{A^+}\right)\right], \quad \text{at} \quad \frac{y}{\delta} < 0.2, \\ L_m^{\text{out}} = 0.085\delta, \quad \text{at} \quad \frac{y}{\delta} > 0.2, \end{gathered} \tag{1.39}$$

where

$$y^+ = \frac{y}{\nu_w}u_\tau = \frac{y}{\mu_w}\rho_w u_\tau = \frac{y}{\mu_w}\sqrt{\rho_w \tau_w} = y\sqrt{\frac{\rho_w}{\mu_w}\left(\frac{\partial u}{\partial y}\right)_w}, \quad u_\tau = \sqrt{\frac{\tau_w}{\rho_w}}, \quad \tau_w = \mu_w\left(\frac{\partial u}{\partial y}\right)_w;$$

δ is the thickness of the dynamic boundary layer; $\chi = 0.4$ is Karman's empirical constant [10]; $A^+ = 26$; and ν_w is the kinematic viscosity near the surface.

In the Baldwin–Lomax model [7, 8], the two-layer structure of the turbulent boundary layer is also considered. In the inner layer adjacent to the surface

$$\mu_{t,\text{in}} = \rho(\chi y D)^2 |\Omega| = \rho\left\{\chi y\left[1 - \exp\left(-\frac{y^+}{A^+}\right)\right]\right\}^2 |\Omega|, \tag{1.40}$$

where D is the Van Drist damping function.

In the outer layer

$$\begin{gathered} \mu_{t,\text{out}} = KC_{cp}\rho F_{\text{wake}} F_{\text{kleb}}(y), \\ F_{\text{kleb}}(y) = \left[1 + 5.5\left(y\frac{C_{\text{kleb}}}{y_{\max}}\right)^6\right]^{-1}, \quad C_{\text{kleb}} = 0.3, \\ F_{\text{wake}} = y_{\max}F_{\max}, \quad F(y) = y|\Omega| D, \end{gathered} \tag{1.41}$$

where $K = 0.018$, $C_{cp} = 1.6$; $y_{\max}$ is determined by the local coordinate normal to the surface y where $|\Omega|$ reaches its maximum, and $F_{\max} = F(y_{\max})$

The turbulent viscosity can be found from the relation

$$\begin{gathered} \mu_{t,\text{in}}, \quad y \le y_{\text{cross}} \\ \mu_{t,\text{out}}, \quad y > y_{\text{cross}}, \end{gathered}$$

where y_{cross} is the y coordinate at which $\mu_{t,\text{in}} = \mu_{t,\text{out}}$ (at the first time as y increases).

It has been repeatedly noted in [6, 9, 28, 29] that the use of algebraic turbulence models together with the complete Navier–Stokes model faces a number of problems that are absent when solving the problem in the classical boundary layer formulation. In the case of three-dimensional flow around the surface of the descent vehicle, it is not possible to formally distinguish the region of the boundary layer at all points

Table 1. Trajectory parameters of the MSL descent vehicle

t, s	H, km	V_∞, cm/s	ρ, g/cm^3	T_∞, K	α, deg	M
45.1	59.3	5.866×10^5	0.265×10^{-7}	85.7	16.0	30.0
61.5	38.8	5.660×10^5	0.270×10^{-6}	157.0	15.7	28.4
74.0	25.8	4.862×10^5	0.144×10^{-5}	169.8	16.1	23.5
80.5	20.8	4.133×10^5	0.186×10^{-5}	178.9	16.4	19.5
84.7	18.6	3.633×10^5	0.233×10^{-5}	182.7	16.6	16.9

near the surface (for example, in the vicinity of the critical streamline). Therefore, in the practical implementation of algebraic turbulence models, the turbulent viscosity distributions along the local normal to the surface were analyzed and the presence of oscillations of this function after reaching a local maximum was not allowed. This algorithm is considered in detail in [28].

We note one more aspect of algebraic turbulence models based on the use of $|\Omega|$, as the constitutive function of the structure of the vector velocity field. A comparison of this function in the vicinity of the critical streamline and in the region of developed flow near the frontal surface (especially over the leeward side of the frontal shield) shows that they differ by more than two orders of magnitude. The use of algebraic models in the region of the critical streamline practically does not introduce any changes in the numerical solution, since the predicted turbulent viscosity turns out to be noticeably lower than the molecular viscosity. In contrast, over the leeward side of the frontal shield, the value of $|\Omega|$ becomes so significant that the calculated turbulent viscosity exceeds the molecular viscosity by more than two orders of magnitude. Thus, despite the fact that this model does not analyze and does not specify the critical Reynolds number of laminar–turbulent transition, in the numerical solution such a region is obtained automatically depending on the value of $|\Omega|$. Of course, such an effect of applying algebraic models should not be interpreted as an automatic determination of the laminar–turbulent transition zone. Nevertheless, numerous examples of the use of algebraic turbulence models without introducing the critical Reynolds number show a fairly good description of the experimental data. At the same time, nothing prevents the setting of the critical Reynolds number for a more detailed description of the experimental data [28]. By the way, an estimate of the critical Reynolds number for one of the characteristic trajectory points gives $\mathrm{Re}_t \sim 10^6$.

As the boundary conditions for the system of equations (1.1)–(1.5), we used the conditions in the undisturbed freestream flow (see Table 1), the no-slip conditions on the surface, and the Dirichlet conditions in the outlet cross-section of the computational domain, where the flow was always supersonic.

2. ALGORITHMS FOR NUMERICAL INTEGRATION OF THE COMPLETE SYSTEM OF EQUATIONS

When solving the system of Navier–Stokes equations, an explicit integration algorithm was used, and the AUSM algorithm [30] was used to solve the problem of the breakdown of an arbitrary discontinuity on the faces of the computational cells.

The system of energy conservation equations for translational and vibrational degrees of freedom was integrated using the implicit finite-difference method. At each iterative time step, up to obtaining a steady-state solution, a system of 7-point finite-difference equations was solved using the lower and upper relaxation algorithms (the choice of relaxation coefficients was made during the calculation process) with sweeps along the coordinate lines.

During transition from one iterative layer to another, thermodynamic and thermophysical data were calculated, including the calculation by the formulas of algebraic turbulence models.

In the calculations we took into account 6 components of dissociated carbon dioxide (C, O, C_2, O_2, CO, CO_2), 28 chemical reactions and 5 vibrational modes of O_2, CO, CO_2 molecules. All the constants necessary for the calculation were borrowed from [16].

The calculations of radiative heat transfer were carried out using the ASTEROID computer code [31], which makes it possible to determine the spectral optical properties of heated gases and low-temperature plasma in the temperature range of 1000–20000 K in a wide spectral range from the vacuum ultraviolet to the far infrared region. The group radiative functions, in particular, the density of the radiative flux on the surface, were determined by averaging the spectral functions within the limits of the elementary spectral

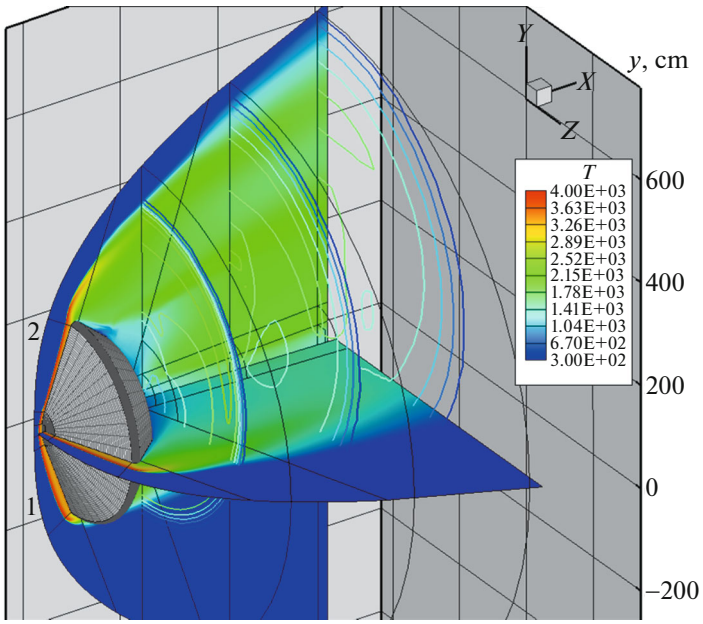

Fig. 1. Temperature field in the vicinity of the MSL descent vehicle at $t = 74$ s.

ranges (spectral groups). The optical properties of carbon dioxide in the infrared region of the spectrum were calculated using the data from [32].

The density of the total heat flux to the surface was determined from the formulas:

$$Q_w = Q_{w,\mathrm{tot}} + Q_{\mathrm{rad}},$$

$$Q_{w,\mathrm{tot}} = Q_{w,\mathrm{hc}} + Q_{\mathrm{dif}} = -\lambda \mathrm{grad}\, T - \rho \sum_{i}^{N_s} h_i D_i \mathrm{grad}\, Y_i,$$

$$Q_{\mathrm{rad}} = \sum_{g=1}^{N_g} Q_{\mathrm{rad},g} = \sum_{g=1}^{N_g} \int_g q_{r,\omega}\, d\omega.$$

3. CALCULATION RESULTS

The calculations were carried out under the free-stream flow conditions given in Table 1 [1]. On the studied, most heat-stressed section of the trajectory, the flight Mach number decreases from 30 to 17. The most intense heating is observed at 74 s of the active deceleration phase, and the highest pressure in the compressed layer is reached at $t = 80.5$ s. The configurations of the fields of gas-dynamic functions are similar at different trajectory points. The general laws of their change consist in the fact that the effects of physicochemical nonequilibrium are manifested to a greater extent at the highest height in the compressed layer. Gas is thermalized noticeably faster as the vehicle slows down and reaches the denser layers of the atmosphere.

For example, we will analyze the fields of gas-dynamic functions near the entry vehicle at the instant of time $t = 74$ s.

Figures 1 and 2 show the temperature distributions of the translational degrees of freedom and the longitudinal flow velocity. The same figures show the surface grid used in the calculations. Note that despite the fact that the nodes of the computational grid are very detailed on the surface and, in particular, on the areas of the surface with the greatest curvature (where a relatively high heating intensity is expected), setting the fine grid along the normal to the surface makes the aspect ratio of elementary computational cells not quite favorable for numerical solution. This necessitates a careful control of the resulting numerical solution through additional numerical experiments.

Figures 1 and 2 clearly show structural features of the solution that are important for the problem being solved. The windward and leeward regions of the flow near the frontal aerodynamic shield are denoted

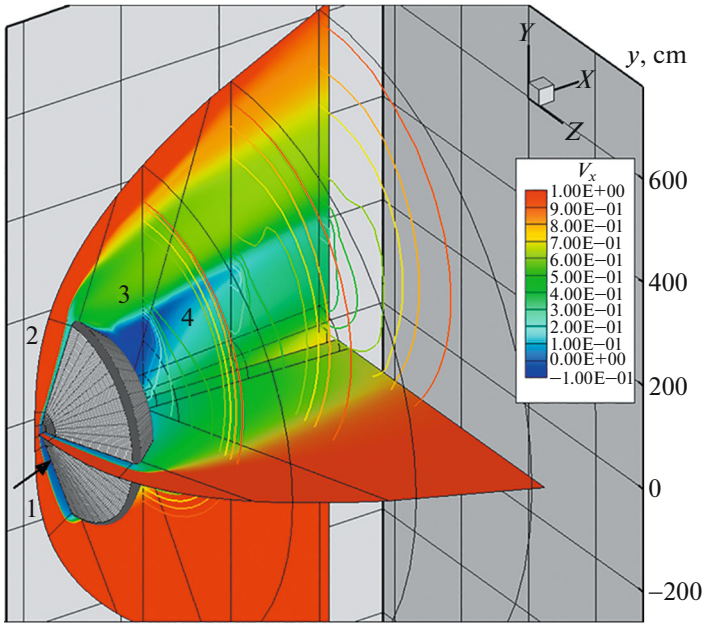

Fig. 2. Longitudinal velocity field $V_x = u/V_\infty$ in the vicinity of the MSL descent vehicle at $t = 74$ s.

by numbers 1 and 2. The location of the critical streamline, from which the gas begins to spread in the compressed layer in all directions, is shown in Fig. 2 by an arrow. In the vicinity of the critical streamline, the gas flow in the compressed layer is subsonic. As the gas spreads along the frontal surface, the velocity increases and becomes supersonic, except for the immediate vicinity of the surface, where it remains subsonic. It can be seen that the thickness of the compressed layer near the windward side of the frontal shield significantly exceeds the thickness of the compressed layer above the leeward side, where the flow is already accelerating to high supersonic speeds. The combination of these properties of the compressed layer well explains the difference in order of magnitude of the velocity vortex function $|\Omega|$ in these regions, which, as noted above, is the main gas-dynamic function that determines the intensity of turbulent mixing in the near-wall boundary layer. Note also that large temperature gradients are observed over the leeward side (see Fig. 1). All of the above largely explains the intensification of heat transfer over the leeward side of the surface.

Of course, the flow structure in the wake (region 3 in Fig. 2) and in the zone of the formed vortex flow (region 4 in Fig. 2) does not have a clear effect on the flow field near the frontal surface. However, these two regions are important for predicting the density of the radiative heat flux on the rear surface of the descent vehicle. It can be seen that the gas temperature in the wake remains very high, of the order of 2000–2500 K. In this case, the hot radiating region has very large dimensions. This leads to the fact that the rear surface is heated by radiation not only from the layers adjacent to the surface, but also from the volumes of heated gas at a distance of tens of meters. The issue of limiting the size of the computational region of the heated gas in the wake was studied earlier [16]. It is shown that under typical conditions of the Martian entry it is necessary to perform calculations up to ~10–20 m from the surface. We can add that the used model for calculating the transfer of selective thermal radiation, which is based on integration of the equation for the radiation transfer along a large number of rays emitted from the surface, makes it possible to take into account reabsorption, which manifests itself to a greater extent in relatively low-temperature layers of the gas (for example, near the surface).

Figures 3 and 4 show the fields of the CO_2 and CO mass number densities. It is these two gas components that play the greatest role in radiant heating of the frontal and rear surfaces. The number density distribution of these elements near the surface is also fundamentally important for determining the diffusion components of total convective flows, which often exceed the thermal conductivity ones.

Figure 3 shows that the free-stream flow of carbon dioxide rapidly dissociates in the compressed layer, especially near the windward side of the surface. Significant gradients of CO_2 mass fractions are also observed over the leeward surface. We also note significant variations in the mass fractions of CO_2 in the separation zone and in the wake, which has a noticeable effect on the intensity of radiant heat transfer.

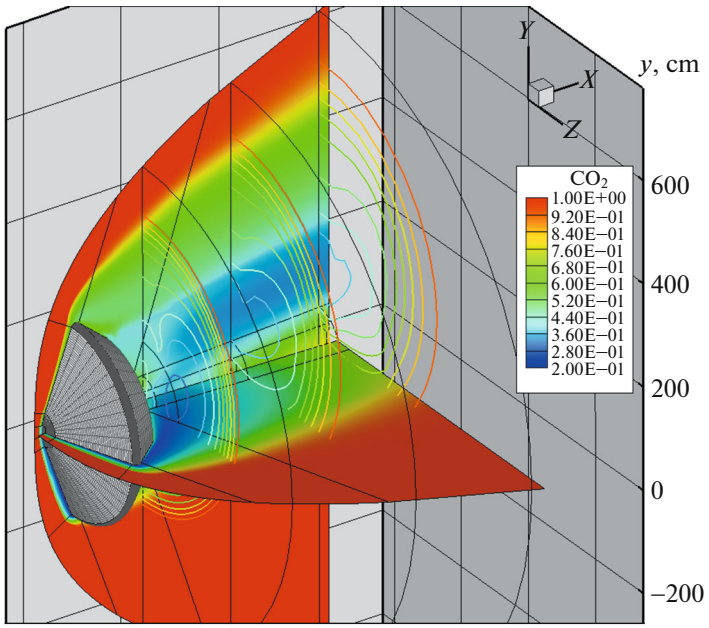

Fig. 3. The field of CO_2 weight fractions in the vicinity of the MSL descent vehicle at $t = 74$ s.

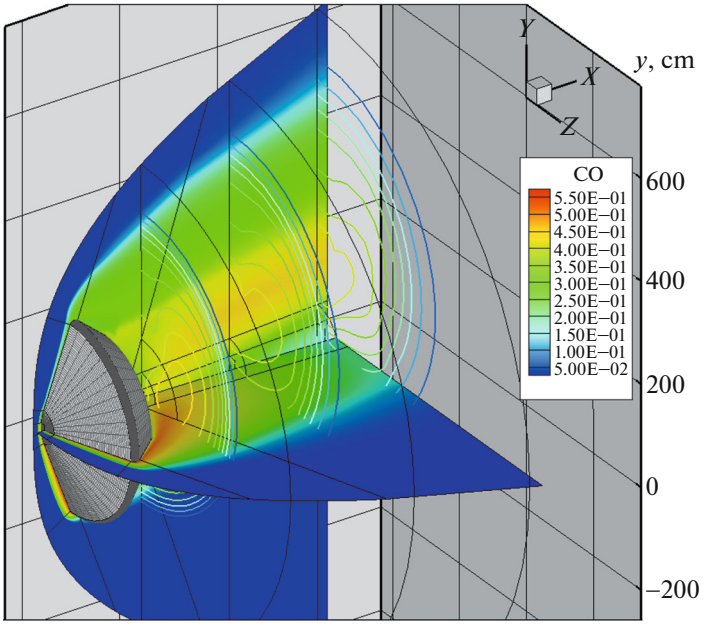

Fig. 4. The field of CO weight fractions in the vicinity of the MSL descent vehicle at $t = 74$ s.

The main product of the dissociation of CO_2 molecules are CO molecules. Figure 4 shows the formation of CO in a compressed layer above the windward and leeward surfaces, as well as their noticeable concentrations in the wake.

Figures 5a, 5b, and 5c show the main results of the study, namely, the convective and integral radiative heat flux distributions along the surface for the trajectory points $t = 65$, 74, and 81 s. In these figures, the frontal shield area extends from ~ –200 to +200 cm, where s is the coordinate reckoned along the surface. All three figures clearly show that the density of the convective heat flux over the leeward side of the frontal shield is several times higher than the flux density on the windward side. These calculations confirm the conclusions of [1] about the presence of significant turbulent heating of the leeward surface. Moreover,

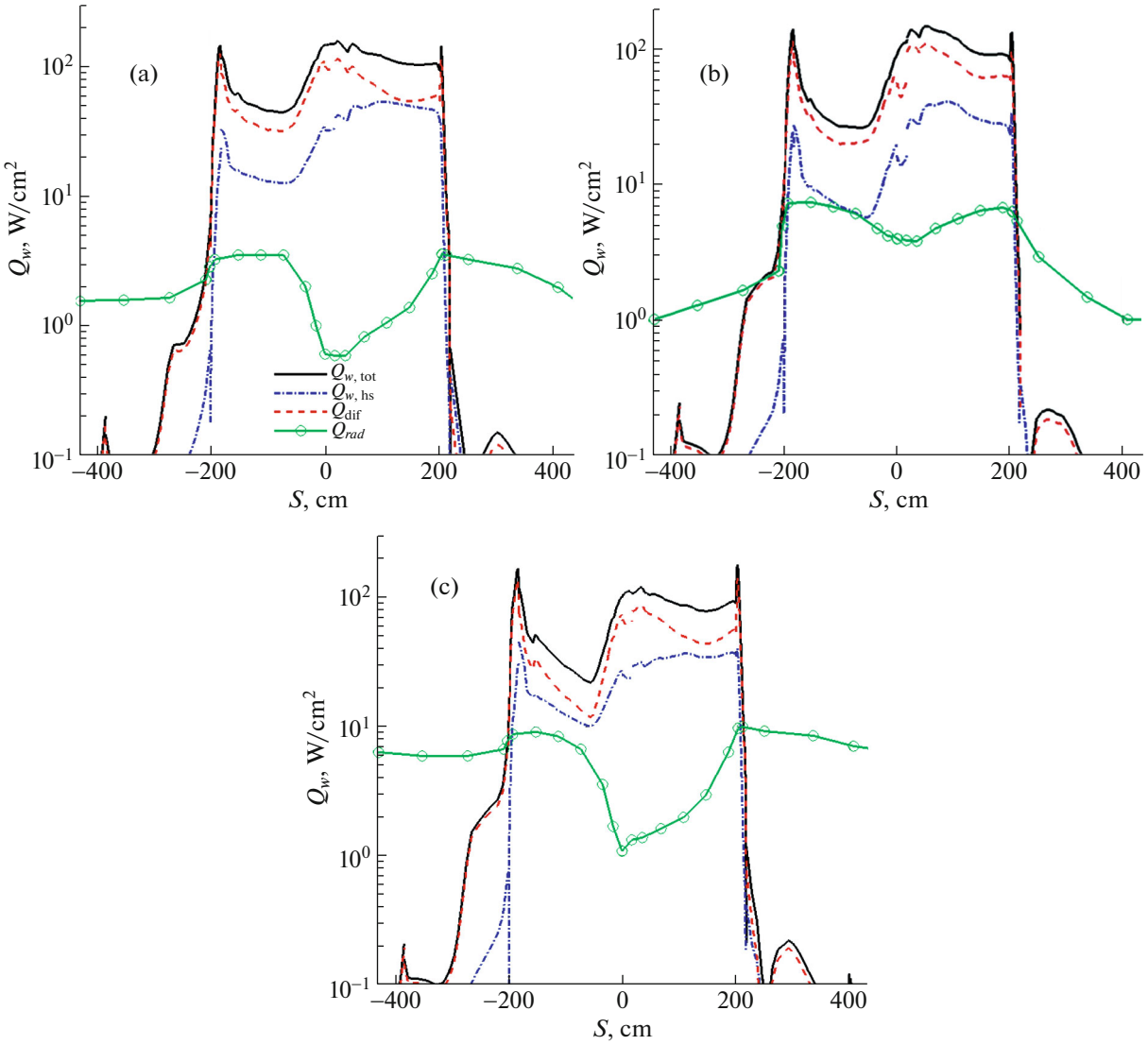

Fig. 5. Density distributions of the convective and integral radiative heat fluxes $Q_{w,\text{tot}} = Q_{w,\text{hc}} + Q_{\text{dif}}$ and Q_{rad} along the surface of the MSL descent vehicle in the plane of symmetry at $t = 65$ s. The Baldwin-Lomax turbulent mixing model. Constant frontal surface temperature $T_w = 1000$ (a), 1500 (b), and 1200 (c).

there is a good quantitative agreement with the calculated data [1], which are shown in these figures by red circles. Note that surface heating due to diffusion heat fluxes is predominant.

The results of the calculations presented in Fig. 5 were performed at fixed surface temperatures (they are indicated in the captions to the figures). In Fig. 6 we have shown the results of calculations of the densities of convective heat fluxes using the model of equilibrium-radiative surface temperature. The change in the density of the convective heat flux in comparison with the case of setting a constant temperature (Fig. 5b) turned out to be insignificant. In this case, the obtained temperature distribution along the surface is shown in Fig. 7.

Variable temperature heat transfer calculations were also performed using the Prandtl mixing model (see Fig. 8). Qualitatively and quantitatively similar results are obtained, as for the Baldwin–Lomax model. There are some differences in the densities of convective heat fluxes for the edge of the aerodynamic shield. However, it should be noted here that the indicated flow area should be studied more carefully, including using specially constructed finite difference grids.

The temperature distributions of translational and vibrational degrees of freedom along the critical streamline (Fig. 9) for three consecutive trajectory points demonstrate a rapid thermalization of the flow

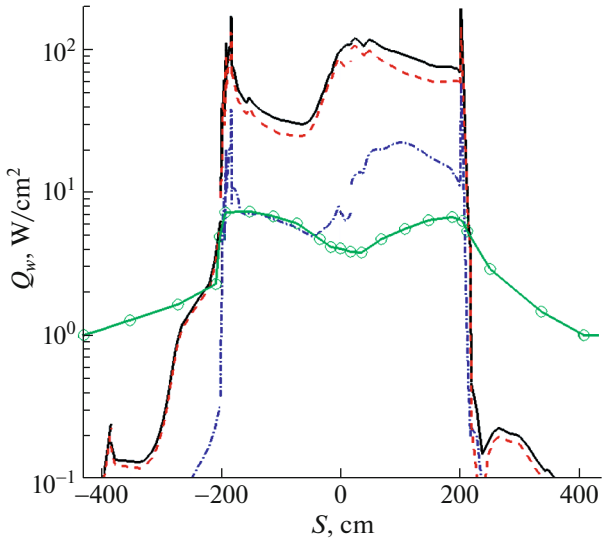

Fig. 6. Density distribution of the convective and integral radiative heat fluxes $Q_{w,\text{tot}} = Q_{w,\text{hc}} + Q_{\text{dif}}$ and Q_{rad} along the surface of the MSL descent vehicle in the plane of symmetry at $t = 74$ s. The Baldwin–Lomax turbulent mixing model. The equilibrium – radiation surface temperature.

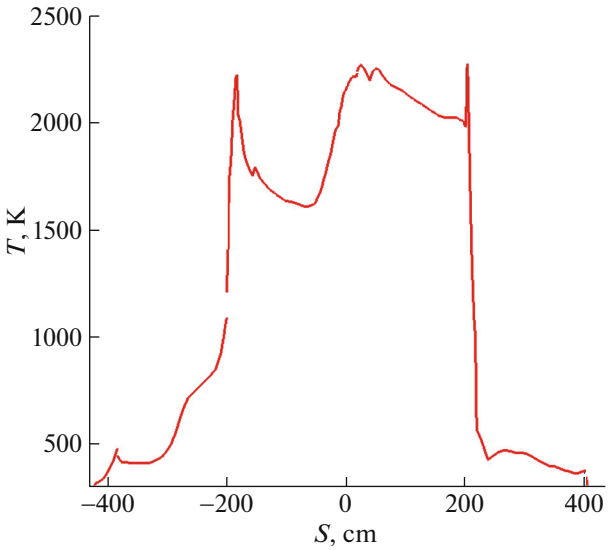

Fig. 7. Equilibrium – radiation surface temperature at $t = 74$ s.

behind the shock wave front. Of course, as the flight altitude increases, the dimensions of the relaxation zone also increase. However, at these points, the intensity of thermal and force action on the surface is much lower.

Figure 10 shows the results of calculations of group radiative heat fluxes and the corresponding cumulative functions at 6 points on the surface. Figure 11 shows the distribution of points of the finite-difference grid along the surface (from the 1st to the 254th). Among the 23 points on the surface marked with rectangles, in which the calculation of the integral radiative heat fluxes was carried out, whose values are shown in Figs. 5 and 6, for 6 points, whose numbers are also given in Fig. 10, the distributions of group spectral fluxes are shown. These distributions, as well as their cumulative functions, show (Fig. 10b) that the main radiative heating is due to radiation in the infrared region of the spectrum. Vibrational-rotational bands of CO_2 and CO molecules are intensively emitted here. Noticeably less intense electronic vibrational bands of CO ($A^1\Pi - X^1\Sigma^+$), C_2 ($C^1\Pi_g - A^1\Pi_u$, $d^3\Pi_g - a^3\Pi_u$, $D^1\Sigma_u^+ - X^1\Sigma_g^+$), and O_2 ($B^3\Sigma_u^- - X^3\Sigma_g^-$)

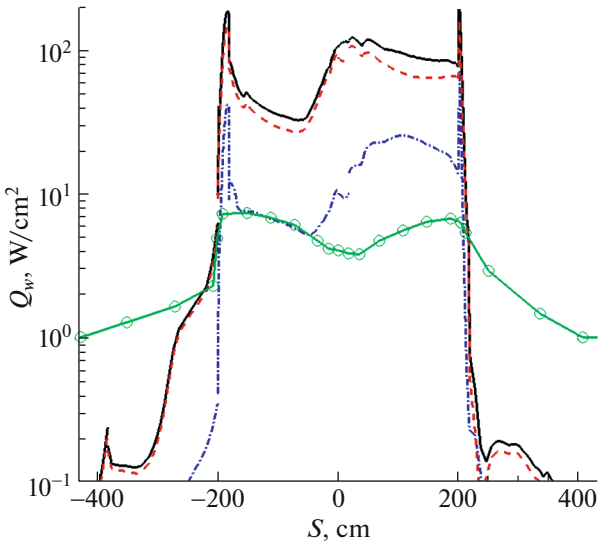

Fig. 8. Density distribution of the convective and integral radiative heat fluxes $Q_{w,\text{tot}} = Q_{w,\text{hc}} + Q_{\text{dif}}$ and Q_{rad} along the surface of the MSL descent vehicle in the plane of symmetry at $t = 74$ s. The Prandtl turbulent mixing model. The equilibrium – radiation surface temperature.

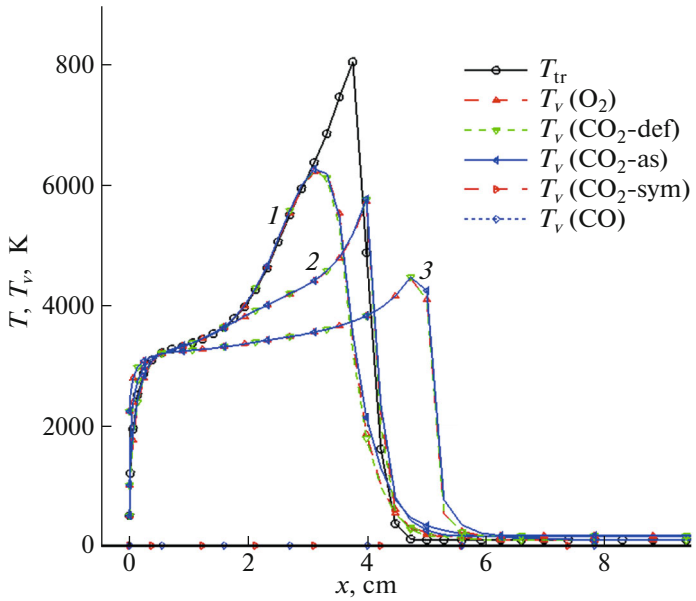

Fig. 9. Distributions of translational and vibrational temperatures along the critical streamline near the MSL descent vehicle surface at $t = 45.1$ (curve *1*), 61.5 (curve *2*), and 74 s (curve *3*).

are observed in the visible region of the spectrum. It should be noted that a more detailed analysis of the composition of the gas near the thermally destroyed surface will undoubtedly introduce its own corrections into the spectral composition of radiative heat fluxes. Nevertheless, the phenomenon of predominant heating of the rear surface of the descent vehicle in the Martian atmosphere, established in [33], will be observed with a high degree of reliability.

4. SUMMARY

The use of the three-dimensional radiation–gasdynamic NERAT-3D model for interpreting the flight data [1] on the thermal load on the MSL descent vehicle during hypersonic braking in the Martian atmo-

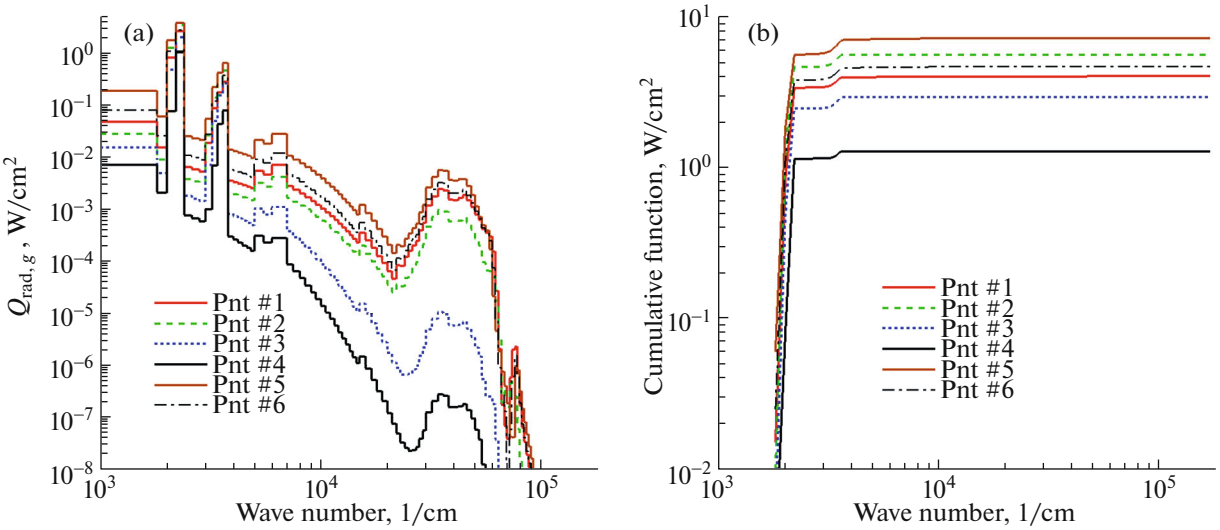

Fig. 10. Spectral distribution of the group densities of radiative heat fluxes (a) and the corresponding cumulative functions (b) at 6 points on the surface of the MSL descent vehicle at $t = 74$ s.

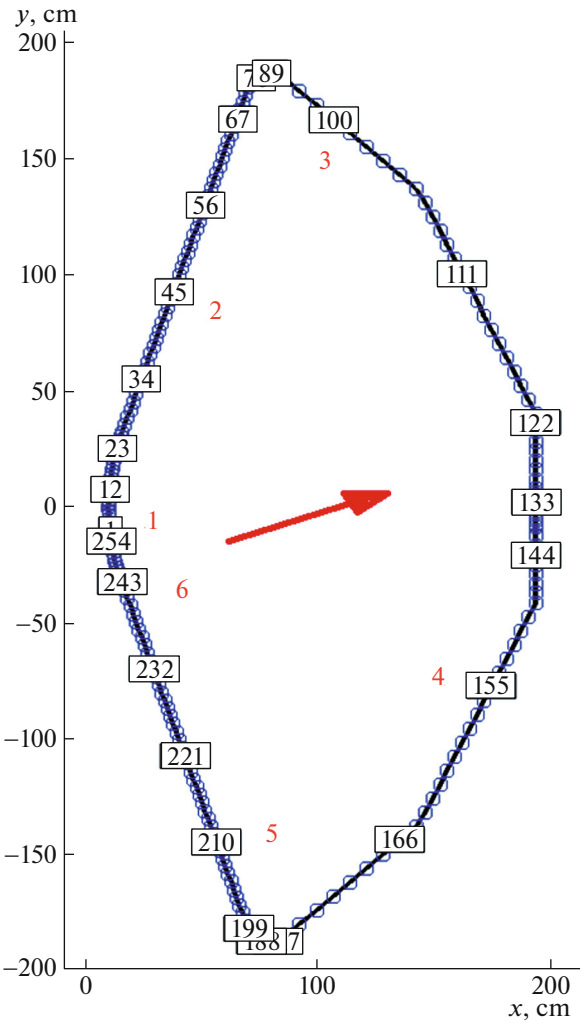

Fig. 11. Coordinates of points on the surface, in which the densities of the integral radiative heat fluxes were calculated. The arrow shows the direction of the free-stream gas flow vector.

sphere confirmed the assumption of heat transfer intensification on the leeward side of the aerodynamic shield, which is most likely associated with laminar–turbulent transition in the near-wall boundary layer as the gas accelerates along the surface. The increase in the density of the convective heat flux on the leeward surface compared to the windward side reaches 3–4 times.

The calculations are performed taking into account non-equilibrium physical and chemical processes in a high-temperature compressed layer using the Reynolds-averaged Navier–Stokes equations together with the Baldwin–Lomax and Prandtl algebraic models of turbulent mixing. A good agreement is shown with the calculated data [1] obtained using the computer codes LAURA and DPLR, which, in turn, demonstrated satisfactory agreement with the flight data on the thermal load on the frontal shield surface of the MSL descent vehicle during descent in the Martian atmosphere.

The calculations were performed in the approximation of a constant and radiation–equilibrium surface temperature.

For individual trajectory points, the data on heating the surface of the descent vehicle by selective thermal radiation emitted by partially dissociated carbon dioxide in the vicinity of the vehicle were obtained. To solve the problem of radiative heating, we used the method of integrating the equation of radiation transfer along optical rays emitted from the surface. The optical model of a high-temperature gas is based on a multigroup approach for calculating the molecular spectrum averaged over the rotational structure. It is shown that the rear surface of the descent vehicle is heated by thermal radiation with a flux density of 1–10 W/cm^2, which is much greater than convective heating.

FUNDING

The work was carried out within the framework of the State task (theme no. AAAA-123021700057-0).

OPEN ACCESS

REFERENCES

1. Edquist, K.T., Hollis, B.R., Johnston, C.O., Bose, D., White, T.R., and Mahzari, M., Mars science laboratory heat shield aerothermodynamics: Design and reconstruction, *JSR,* 2014, vol. 51, no. 4, pp. 1106–1124.
2. *Planetary Mission Entry Vehicles*, NASA SP-20220010761, Ed by K. Parcelo and G. Allen, Version 4.0, 2022, Carol Davies, ELORET Corporation.
3. Edquist, K.T., Dyakonov, A.A., Wright, M.J., and Tang, C.-Y., Aerothermodynamic design of the Mars science laboratory backshell and parachute cone, *AIAA Paper* 2009-4078, June 2009.
4. Cheatwood, F.M. and Gnoffo, P.A., *Users Manual for the Langley Aerothermodynamic Upwind Algorithm* (LAURA), NASA TM-4674, April 1996.
5. Wright, M.J., Candler, G.V., and Bose, D., Data-parallel line relaxation method for the Navier–Stokes equations, *AIAA J.*, 1998, vol. 36, no. 9, pp. 1603–1609.
6. Surzhikov, S.T., Analysis of the experimental data on the convective heating of a model Martian entry vehicle using algebraic turbulence models, *Fluid Dyn.,* 2019, vol. 54, no. 6, pp. 863–874. https://doi.org/10.1134/S0015462819060119
7. Baldwin, B.S. and Lomax, H., Thin layer approximation and algebraic model for separated turbulent flows, *AIAA Paper* 78–0257, 1978.
8. Visbal, M. and Knight, D., The Baldwin–Lomax turbulence model for two-dimensional shock-wave/ boundary-layer interaction, *AIAA J.*, 1984., vol. 22, no. 7, pp. 921–928.
9. Tannehill, J.C., Anderson, D.A., and Pletcher, R.H., *Computational Fluid Mechanics and Heat Transfer*, Taylor and Francis, 1997.
10. Schlichting, H., *Boundary Layer Theory,* New York: McGraw-Hill, 1968.
11. Surzhikov, S.T., Radiative-convective heating of Martian space vehicle MSL EDL at an angle of attack, *Fiz.-Chem. Kinet. Gas. Din.*, 2015, vol. 16, no. 2. http://chemphys.edu.ru/issues/2015-16-2/articles/604/

12. Surzhikov, S.T., Three-dimensional computer model of nonequilibrium aerophysics of the spacecraft entering in the Martian atmosphere, *Fluid Dyn*., 2011, vol. 46, no. 3, pp. 490–503.
13. Surzhikov, S.T., Comparative analysis of radiative aerothermodynamics of Martian entry probes, *AIAA paper*, AIAA 2012-2867, 2012.
14. Surzhikov, S.T., Radiative-convective heating of Martian probes, *Fiz.-Chem. Kinet. Gas. Din*., 2013, vol. 14, no. 2. http://chemphys.edu.ru/issues/2013-14-2/articles/408/
15. Surzhikov, S.T., Numerical analysis of shock layer ionization during the entry of the *Schiaparelli* spacecraft into the Martian atmosphere, *Fluid Dyn.,* 2020, vol. 55, no. 3, pp. 364–376. https://doi.org/10.1134/S001546282003012X
16. Surzhikov, S.T., *Radiatsionnaya gazovaya dinamika spuskaemykh kosmicheskikh apparatov. Mnogotemperaturnye modeli* (Radiative Gas Dynamics of Entry Spacecraft. Multi-Temperature Models), Moscow: Institute for Problems in Mechanics of the Russian Academy of Sciences, 2013.
17. Stupochenko, E.V., Losev, S.A., and Osipov, A.I., *Relaksatsionnye protsessy v udarnykh volnakh* (Relaxation Processes in Shock Waves), Moscow: Glav. Red. Fiz.-Mat. Lit., 1965.
18. Park, C., *Nonequilibrium Hypersonic Aerothermodynamics*, New York: Wiley, 1990.
19. Millikan, R.C. and White, D.R., Systematic of vibrational relaxation, *J. Chem. Phys.*, 1963, vol. 39, no. 12, pp. 3209–3212.
20. Treanor, C.E. and Marrone, P.V., Effect of dissociation on the rate of vibrational relaxation, *Phys. Fluids*, 1962, vol. 5, no, 9, pp. 1022–1026.
21. Bird, R.B., Stewart, W.E, and Lightfoot, E.N., *Transport Phenomena*, New York: Wiley, 2007.
22. Ginzburg, I.P., *Teoriya soprotivleniya i teploperedachi* (Theory of Resistance and Heat Transfer), Leningrad: Izd-vo Leningradskogo Univ., 1979.
23. Svehla, R.A., Estimated viscosities and thermal conductivities of gases at high temperatures, *NASA TR-R-132.* 1962.
24. Wilke, C.R., Diffusional properties of multicomponent gases, *Chem. Eng. Progress,* 1950, vol. 46, no. 2, pp. 95–104.
25. Anfimov, N.A., Laminar boundary layer in a multicomponent gas mixture, *Izv. Akad. Nauk SSSR, Mekh. Mashinost.*, 1962, no. 1, pp. 25–31.
26. Surzhikov, S.T., *Teplovoe izluchenie gazov i plazmy* (Thermal Radiation of Gases and Plasma), Moscow: Izd-vo MGTU im. Baumana, 2004.
27. Zemlyanskii, B.A., Lunev, V.V., Vlasov, V.I. et al., *Konvektivnyi teplobmen letatel'nykh apparatov* (Convective Heat Transfer of Vehicles), Moscow: Fizmatlit, 2014.
28. Surzhikov, S.T., Results of the use of algebraic turbulence models within the framework of the RANS-model of heating a sharp plate surface in supersonic flow, *Fiz.-Chem. Kinet. Gas. Din*., 2023, vol. 20, no. 4. http://chemphys.edu.ru/issues/2023-24-3/articles/1056/
29. Shang, J. S. and Scherr, S. J., Navier – Stokes solution for a complete re-entry configuration, *J. Aircraft*, 1986, vol. 23, no. 12, pp. 881–888.
30. Liou, M.-S., A sequel to AUSM: AUSM+, *J. Comput. Phys*., 1996, vol. 129, pp. 364–382.
31. Surzhikov, S.T., *Opticheskie svoistva gazov i plazmy* (Optical Properties of Gases and Plasma), Moscow: Izd-vo MGTU im. Baumana, 2004.
32. Ludwig, C.B., Malcmus, W., Reardon, J.E., et al., *Handbook of Infrared Radiation From Combustion Gases,* NASA SP-3080, Washington: Marshal Space Flight Center, 1973.
33. Gromov, V.G., Surzhikov, S.T., and Charbonnier. J.-M., Convective and radiative heating of a Martian space vehicle base surface, in: *Proceeding of the 4th European Symposium on Aerothermodynamics for Space Vehicles, Oct. 15–18, 2001, Capua, Italy*. ESA SP-487, 2002, pp. 265–269.

Translated by E.A. Pushkar